



# Interplate coupling and a recent aseismic slow slip event in the Guerrero seismic gap of the Mexican subduction zone, as deduced from GPS data inversion using a Bayesian information criterion

Shoichi Yoshioka<sup>a,\*</sup>, Takeshi Mikumo<sup>b</sup>, Vladimir Kostoglodov<sup>b</sup>,  
Kristine M. Larson<sup>c</sup>, Anthony R. Lowry<sup>d</sup>, Shri K. Singh<sup>b</sup>

<sup>a</sup> Department of Earth and Planetary Sciences, Faculty of Sciences, Kyushu University, Hakozaki 6-10-1, Higashi ward, Fukuoka 812-8581, Japan

<sup>b</sup> Instituto de Geofísica, Universidad Nacional Autónoma de México, Ciudad Universitaria, Del. Coyoacán, 04510 México D.F., México

<sup>c</sup> Department of Aerospace Engineering Science, University of Colorado, Boulder, CO 80309-0429, USA

<sup>d</sup> Department of Physics, University of Colorado, Boulder, CO 80309-0390, USA

Received 22 November 2003; received in revised form 20 May 2004; accepted 20 May 2004

## Abstract

A large-scale slow slip event with a magnitude equivalent to  $M_w = 7.4$  has been observed at seven continuous GPS stations located in the Guerrero–Oaxaca region, southern Mexico, for several months from late 2001 to middle 2002 [Geophys. Res. Lett. (2003) 30: doi: 10.1029/2003GL017219]. We re-analyzed the GPS time series data to estimate the displacements associated with the slow slip event and also the displacement rates during the interseismic period prior to this event, by applying an inversion technique using a Bayesian information criterion (ABIC). We then carried out GPS data inversion again with ABIC and some detailed forward modeling to obtain spatial distributions of the back-slip rates and the slow slip on a 3-D curved plate interface between the subducting Cocos and the overriding North America plates. The results show that the average direction of the back-slip rates is  $N31.3^\circ E \pm 5.6^\circ$ , which is congruent with that of plate convergence in this region. Interplate coupling is found to be very strong down to a depth of about 45 km, indicating a coupling ratio of 0.83–0.86 except for a couple of segments on the model region, and decreases dramatically down below. The average direction of the slow slip is oriented about  $20^\circ$ – $35^\circ$  counterclockwise from the opposite direction of the plate convergence. The slow slip detected on the mid-depth segment to the upper rim of the model region reaches about 9–18 cm in the landward region of the Guerrero seismic gap from inversion and forward modeling. From these results, we conclude it is possible that the slow slip may have invaded a deeper part of the strongly coupled, seismogenic zone at least up to a depth of about 25 km. We also estimate stress changes due to the slow slip event. Some decrease in shear stress on the plate interface at these depths suggests that if such a slow slip event occurred episodically, it is possible that the time of occurrence of a forthcoming large earthquake in the Guerrero gap would be delayed to some extent.

© 2004 Elsevier B.V. All rights reserved.

**Keywords:** ABIC; GPS data inversion; Forward modeling; Interplate coupling; Aseismic slow slip event; Aseismic slip on the seismogenic zone; Guerrero seismic gap

\* Corresponding author. Tel.: +81 92 642 2646; fax: +81 92 642 2684.  
E-mail address: [yoshioka@geo.kyushu-u.ac.jp](mailto:yoshioka@geo.kyushu-u.ac.jp) (S. Yoshioka).

## 1. Introduction

In the Pacific coast of southern Mexico, a number of large to great thrust earthquakes ( $M_w > 7$ ) have taken place quite frequently due to the subduction of the Cocos and Rivera plates beneath the continental North America plate along the Middle America trench. Seismotectonic features of this subduction zone appear to be segmented into five regions; the Jalisco-Colima, Michoacan, Guerrero, Oaxaca and Chiapas regions, which are bounded by the Rivera fracture zone, the East Pacific rise, the Orozco and O’Gorman fracture zones, and the Tehuantepec ridge (Singh and Mortera, 1991) (Fig. 1). The rate and direction of plate convergence along this zone between  $98^\circ\text{W}$  and  $102^\circ\text{W}$  are estimated to be in the range from 5.3 to 6.3 cm/year and  $\text{N}35^\circ\text{E}$ , respectively, based on the NUVEL-1A global plate motion model (DeMets et al., 1994). The plate convergence could provide stress accumulation leading to major earthquakes along this zone at the recurrence time interval of a few to several tens of years.

The northwestern Guerrero region, however, has experienced no major earthquakes since a large earthquake ( $M_s = 7.6$ ) in 1911, and hence is called the Guerrero seismic gap, which extends for a length of about 200 km between  $99.2^\circ\text{W}$  and  $101.2^\circ\text{W}$ . If this seismic gap was ruptured in a single earthquake, its magnitude would be  $M_w = 8.1\text{--}8.4$  (Suárez et al., 1990; Singh and Mortera, 1991), which is large enough to provide heavy damage not only in the state of Guerrero, but in Mexico city. It is thus extremely important to perform continuous monitoring for stress accumulation and seismogenic potential in this region.

For this purpose, eight permanent GPS stations have been established up to this time in and around the Guerrero region, implemented by more than 20 campaign sites, since the first, continuous GPS receiver was installed at the CAYA station in 1997 (Lowry et al., 2001; Larson et al., 2004). The GPS observations at CAYA first recorded a transient displacement in early 1998, which had a reverse sense to that expected from plate convergence, and has been interpreted as due to an anomalous, slow slip event

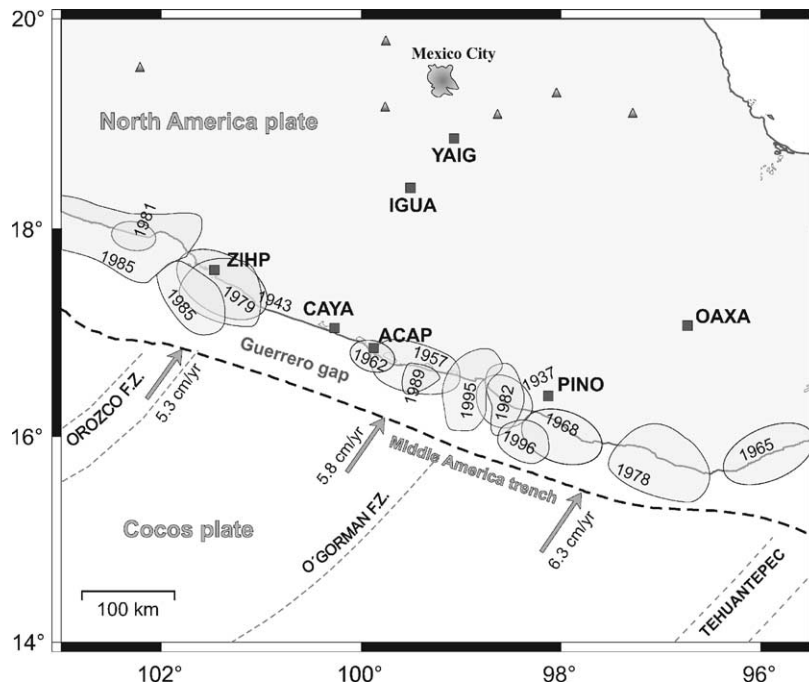


Fig. 1. A tectonic map and source areas of large subduction earthquakes in southern Mexico. Solid squares show the locations of continuous GPS stations. Solid triangles denote the locations of active volcanoes. The arrows indicate the convergence rates and their directions of the Cocos plate relative to the North America plate along the Middle America trench.

propagated on the upper plate interface horizontally (Lowry et al., 2001). An aseismic slow slip event was again observed during November–December 2001 to April 2002 at four GPS stations in the central part of the Guerrero region, and from January–February to May 2002 at three stations located outside the region (Kostoglodov et al., 2003). Similar aseismic slow slip events have been observed in some other subduction zones such as around the Japanese Islands (e.g., Hirose et al., 1999; Ozawa et al., 2001, 2002, 2003) and in the Cascadia region, Canada (Dragert et al., 2001), but their extent of the area is much limited than in the present case.

The Guerrero observations have been modeled by a 2-D dislocation on the plate interface with a curved, shallow part and a deeper, subhorizontal part located in an elastic half space (Kostoglodov et al., 2003). They proposed two extreme models; one model assumes slow slip occurring over the entire portion of the modeled interface including a shallow seismogenic zone. In this case, shear stress accumulated during the interseismic phase will decrease on most part of the interface and thus would delay the time of a next large earthquake. The other model assumes the slow slip on a deeper transitional interface, remaining the shallow seismogenic zone locked. In this second case, shear stress accumulated on the shallow seismogenic zone will increase and thus may accelerate the time of the next earthquake. Accordingly, stress changes due to the slow slip event are crucial to understand the state of seismogenic potential in this region. Although the above calculations are based on 2-D forward modeling, the slow slip event is also being analyzed by a 3-D dislocation model for two planar faults with a nonlinear, simulated annealing inversion technique (Iglesias et al., 2004).

In the present study, we perform more detailed analysis with both inversion and forward modeling of the processed GPS data for a more feasible 3-D plate interface based on isodepth contours of the subducting Cocos plate (Pardo and Suárez, 1995). The main purpose here is to estimate the amount and direction of interplate coupling during the interseismic period, the slip distribution of the aseismic slow slip event, and the change of shear stress, and to clarify their relationship and seismotectonic implications, especially in relation to seismic potential in the Guerrero seismic gap.

## 2. Analysis of GPS data

### 2.1. Processing of GPS data

The observed GPS data have been analyzed by Larson et al. (2004) with GIPSY-OASIS software package (Lichten and Border, 1987), in which IGS orbits were referred to the satellite coordinates in the ITRF2000 reference frame (Boucher et al., 1999). During this procedure, receiver coordinates, clock values and zenith tropospheric delays have been corrected using standard estimation strategies. All the data sampled at every 30 s were converted into a series of one estimate per day by the weighted least squares analysis (Larson et al., 2004). The reference point is taken at MacDonal GPS station in Texas, which is considered to be located in a stable region on the North America plate.

### 2.2. Estimate of displacement rates during interseismic period and displacements associated with an aseismic slow slip event at GPS stations using a Bayesian approach

The time series thus obtained for the NS, EW, and UD components of GPS data at CAYA, ACAP, and IGUA stations are shown in Fig. 2. At the CAYA and ACAP stations, we find that northward, eastward, and downward movements during the period from mid-1998 to late 2001. Since the two stations are located at the Pacific coast in the Guerrero region (Fig. 1), these movements can be regarded as a result of dragging of the overriding North America plate associated with the subduction of the Cocos plate during an interseismic period. However, from the end of 2001 to middle 2002, such movements changed their direction to the opposite sense on all the three components at the two stations. Since this change has been detected at the rest of the five GPS stations, the movements toward the opposite directions can be regarded as being produced by an aseismic slow slip on the plate interface. After the period, another interseismic phase appears to restart, as can be seen in Fig. 2. It could be seen on the CAYA record that the smaller slow slip event occurred at the beginning of 1998, as investigated by Lowry et al. (2001).

Since the time series include observation errors, annual and semi-annual variations, and missing data, we

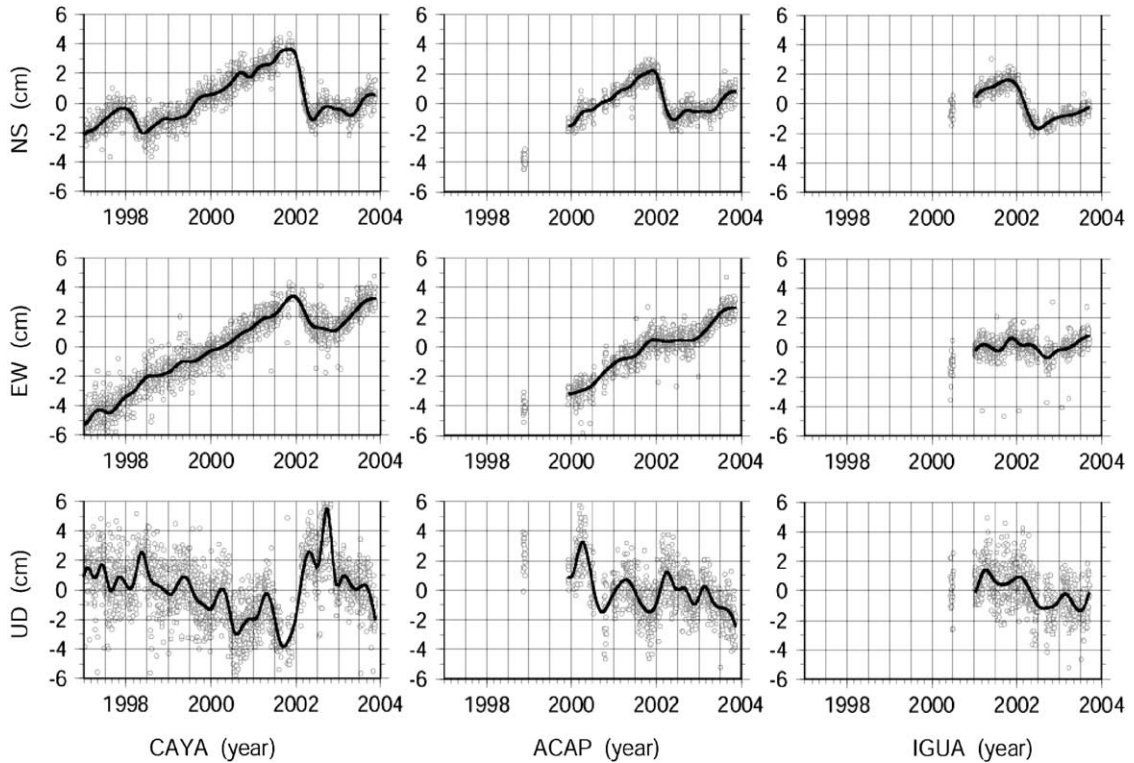


Fig. 2. Observed time series GPS data (gray open circles). Solid curves show “the best fit curves”, which were obtained by the method described in Section 2.2. Left panel: time series at CAYA station. Top: displacements in the NS component. Positive and negative values indicate northward and southward displacements, respectively. Middle: displacements in the EW component. Positive and negative values indicate eastward and westward displacements, respectively. Bottom: displacements in the UD component. Positive and negative values indicate upward and downward displacements, respectively. Middle panel: time series at ACAP station. Top: NS component. Middle: EW component. Bottom: UD component. Right panel: time series at IGUA station. Top: NS component. Middle: EW component. Bottom: UD component.

need to correct the data appropriately and use an objective and unique method to estimate the displacement rate during the interseismic period and the amount of the aseismic slip for each component as rigorously as possible. For this purpose, we employed the following two procedures:

1. To obtain “a best fit curve” to explain the time series for each component.
2. For “the best fit curve” for each component, we estimate a linear trend during the interseismic period and the amount of slow slip, taking account of annual and semi-annual variations.

In the first procedure, in order to obtain “a best fit curve” for the time series data with noise and its

missing portion, we applied a method proposed by Tanabe (1985).

We briefly explain the method here. In general, there are two extreme cases to explain time series data. One is a curve to pass through all the observed data, and the other is a linear least squares fitting, both of which are considered inappropriate: in the first case, since the data include noise, the curve does not represent a true structure of the time series data. In the second case, we will lose useful information hidden in the data. Also there is no reason to apply trigonometric functions or a function with higher-order time terms to the data. One of the most suitable assumptions would be that the time series data are smooth to some degree. From this viewpoint, the first case is the roughest curve, and the

second one is the smoothest curve. The smoothness of the curve can be represented by

$$\nabla^2 y(t), \quad (1)$$

where  $t$  is time, and  $y(t)$  is a function representing the curve. Our problem is to determine optimal smoothness for the time series. As a criterion to determine an optimal smoothness of the curve, we use a Bayesian information criterion (ABIC) based on entropy maximization principle (Akaike, 1980). This method is very powerful to extract hidden and useful information from data with noise and missing data. In this study, we used 40 cubic B-spline functions as basis functions and determined their coefficients to obtain “the best fit curve” uniquely and objectively by using an inversion method for each component at the CAYA station. We applied the same method to each component at the other six stations to obtain “the best fit curve”. For the time series with shorter time intervals, we reduced the number of unknown coefficients of the basis functions in proportion to the data length. The curves thus obtained at the CAYA, ACAP, and IGUA stations are drawn in Fig. 2, whose functions are hereafter referred to as  $y_1(t)$ . From these curves, we can find some characteristics of the time series data; the time to change the above-mentioned trend clearly, and annual and semi-annual variations in the UD component much larger than those for the NS and EW components.

As the second procedure, we assume the following equation during the interseismic period and apply it to “the best fit curve”  $y_1(t)$ :

$$y_2(t) = a + bt + y_3(t), \quad (2)$$

with

$$y_3(t) = c \sin\left(\frac{2\pi t}{365}\right) + d \cos\left(\frac{2\pi t}{365}\right) + e \sin\left(\frac{4\pi t}{365}\right) + f \cos\left(\frac{4\pi t}{365}\right), \quad (3)$$

where in the right side of Eq. (2), the first and second terms represent a linear trend. The first and second terms in the right side of Eq. (3) are annual variations, and the third and fourth terms are semi-annual variations. The unknown six coefficients  $a$ – $f$  can be determined by the least squares method for each component. The reason why we did not apply this equation

directly to the original time series data is that the data include noise and missing portions, resulting in erroneous estimate of these coefficients. By determining the coefficient  $b$  in Eq. (2), we can estimate the displacement rate for each component during the interseismic period.

The linear trends thus estimated for the three stations are shown in Fig. 3, together with the time series excluding the annual and semi-annual variations  $y_3(t)$  during the interseismic period and its successive period for the slow slip event. We also calculate standard deviations for the corrected data for the purpose of determining a weight of data to be applied in our inversion analysis of the GPS observations, which will be described in the next section.

Since Eq. (2) can be only applied to the data during the interseismic period, we need to use a different function to estimate slow slip displacements for each component. For this purpose, we assumed that the same annual and semi-annual variations during the interseismic period were also included in the time series data for the period of the slow slip event. Then, we employed a function  $y_1(t)$ – $y_3(t)$  to estimate the slow slip displacement, and read a peak-to-peak value for the function even if the terminating time does not coincide each other for the three components at a station, as shown in Fig. 3. For the UD component at CAYA, we adopted the time of the first peak around April in 2002. If we adopt the maximum peak around August in 2002, the uplift reaches 9.3 cm. This approach may be useful especially for the case where the onset and terminating times of the slow slip phase almost coincide with the peak and trough of the large annual and semi-annual variations, as appeared in the UD component at CAYA (Fig. 2). In other words, in this case if we simply regarded a peak-to-peak value of  $y_1(t)$  as the amount of slow slip, it would result in overestimate of its amount. Although detrended time series are customarily used to estimate the amount of slow slips, we avoided applying this method to the data. This is because the estimated amount of slow slip by the method depends on the estimated linear trend during an interseismic period, increasing uncertainty to estimate the amount. Another reason is that the estimated value tends to overestimate the amount of slow slip because steady state motion is assumed even for the period when a slow slip event occurs.

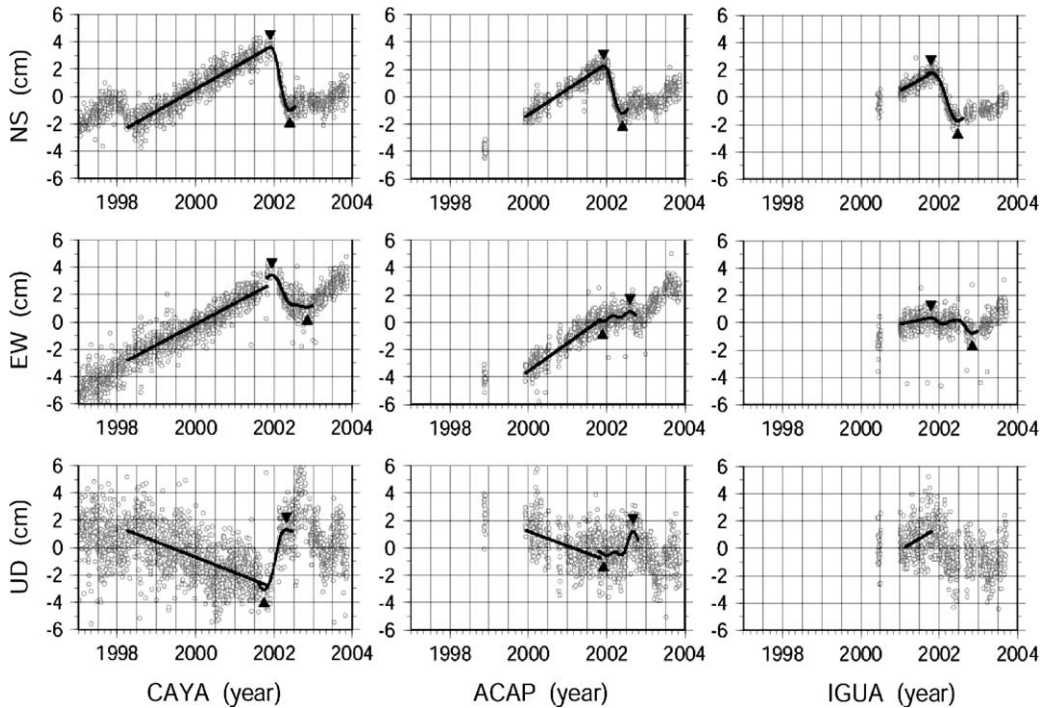


Fig. 3. Corrected time series for the observed GPS data (gray open circles). Annual and semi-annual variations are excluded from the original time series data given in Fig. 2 from a period from spring in 1998 to the end of the slow slip event. The straight line indicates a linear trend during the interseismic period, which was obtained by the method described in Section 2.2. The curved line is drawn to identify peak-to-peak value of the amount of slow slip whose timings are shown by solid triangles. Others are the same as in Fig. 2.

In order to determine a weight of the data, we used standard deviations of the linear trend, which was determined by the least squares method for the function  $y_1(t)$ – $y_3(t)$  for the period of the slow slip event. However, even if we used this approach, we could not estimate the amounts of slow slips for the UD component at stations except for CAYA, ACAP and PINO. This is mainly due to the lack of data lasting for long periods, large standard deviations, and a shorter period of the aseismic slow slip event. The obtained values are listed in Table 1.

### 2.3. Characteristics of spatial distributions of displacement rates during interseismic period and displacements associated with the aseismic slow slip event at GPS stations

Fig. 4 shows the horizontal and vertical displacement rates, by solid arrows and vertical bars, obtained at the seven permanent GPS stations, whose values

have been determined in the previous section. Standard deviation ( $1\sigma$ ) is also shown as an ellipse and a circle for the horizontal and vertical displacement rates, respectively, at each station. We find northeastward horizontal displacement rates at all the stations. The estimated horizontal displacement rates range from 2.2 to 2.8 cm/year at four stations located along the Pacific coast, and decreases toward the inland region except for OAXA. Vertical displacement rates indicate subsidence at three stations located along the Pacific coast, ranging from  $-0.6$  to  $-1.2$  cm/year except for ZIHP. These characteristics can be regarded as a result of dragging of the North America plate due to the subduction of the Cocos plate during the interseismic period. Standard deviations of the horizontal displacement rates are smaller than those of the vertical displacement rates at all the stations, as can be seen from the corrected time series in Fig. 3.

Horizontal and vertical displacements associated with the aseismic slow slip event are represented by

Table 1

Displacement rates for the interseismic period and the displacement associated with the slow slip event for three components at seven permanent GPS stations in southern Mexico

Station	Displacement rate for interseismic period			Displacement associated with the slow slip event		
	$\Delta N$ (cm/year)	$\Delta E$ (cm/year)	$\Delta Z$ (cm/year)	$\Delta N$ (cm)	$\Delta E$ (cm)	$\Delta Z$ (cm)
CAYA	$1.61 \pm 0.50$	$1.52 \pm 0.63$	$-1.12 \pm 1.55$	$-4.61 \pm 0.38$	$-2.34 \pm 0.71$	$4.41 \pm 1.99$
ACAP	$1.86 \pm 0.43$	$2.04 \pm 0.61$	$-1.06 \pm 1.28$	$-3.45 \pm 0.42$	$0.76 \pm 0.61$	$1.68 \pm 1.19$
IGUA	$1.60 \pm 0.35$	$0.57 \pm 0.67$	$1.70 \pm 1.24$	$-3.54 \pm 0.40$	$-0.27 \pm 0.70$	–
YAIG	$0.85 \pm 0.35$	$0.74 \pm 0.56$	$-0.48 \pm 1.28$	$-1.68 \pm 0.30$	$-0.32 \pm 0.45$	–
ZIHP	$2.10 \pm 0.42$	$1.89 \pm 0.67$	$0.01 \pm 1.22$	$-1.05 \pm 0.41$	$0.11 \pm 0.47$	–
PINO	$2.28 \pm 0.40$	$1.46 \pm 0.59$	$-0.59 \pm 1.13$	$-1.57 \pm 0.49$	$-0.62 \pm 0.71$	$1.46 \pm 1.21$
OAXA	$1.97 \pm 0.36$	$1.61 \pm 1.43$	$0.83 \pm 1.10$	$-0.84 \pm 0.36$	$-1.13 \pm 0.70$	–

These values are taken relative to those at MacDonald station in Texas, which is considered to be located in a stable region on the North America plate. Uplift is taken positive for  $\Delta Z$  component. The  $\Delta Z$  components for which reliable values could not be obtained are shown by horizontal bars.

solid arrows and vertical bars in Fig. 5. In contrast to the results for the interseismic period, the directions of the displacements are almost opposite to those in Fig. 4 both in the horizontal and vertical displacements at all the stations. We find southeast to

southwestward horizontal displacements at these stations, which are somewhat rotated counterclockwise from the exact opposite direction of the plate convergence. Unlike the case for the interseismic period, the amount of displacements varies at the four stations

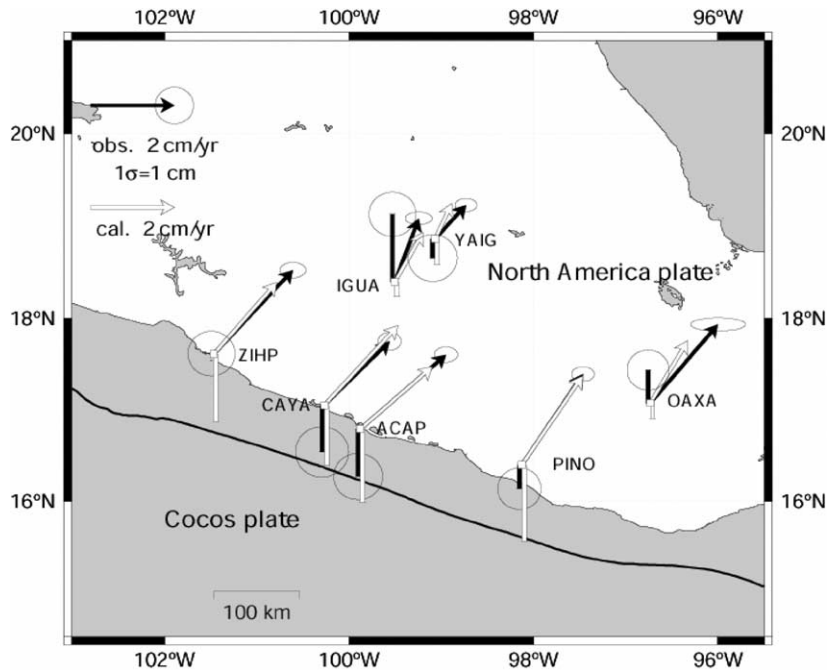


Fig. 4. The observed horizontal (solid arrows) and vertical (solid vertical bars) displacement rates during the interseismic period with their standard deviations (ellipses and circles) at seven GPS stations, comparing with the corresponding displacement rates (open arrows and vertical bars) calculated from the estimated back-slip rates in Fig. 6. Thick upward and downward vertical bars standing at an open square (station location) represent the uplift and subsidence rates, respectively. The scale of the vertical displacement rates is the same as that of the horizontal ones.

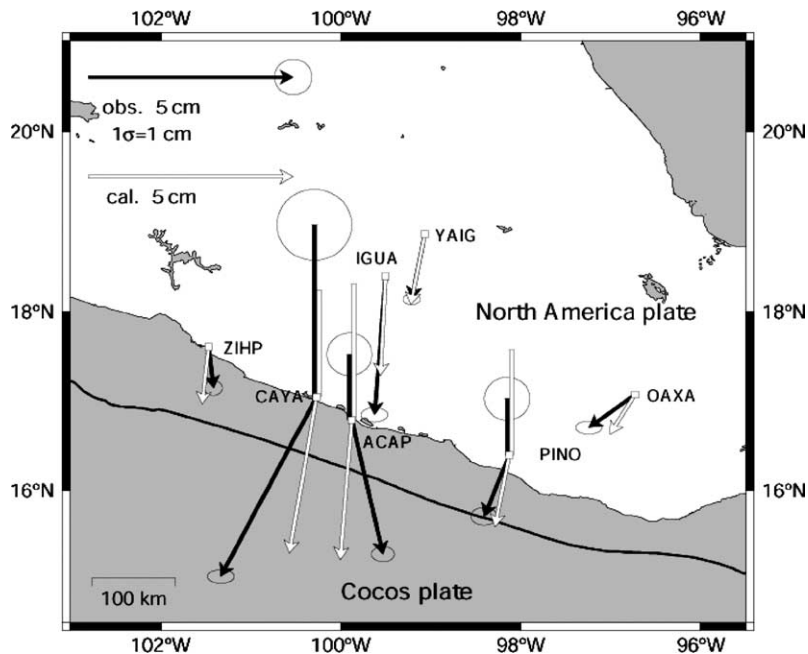


Fig. 5. The observed horizontal (solid arrows) and vertical (solid vertical bars) displacements associated with the slow slip event with their standard deviations (ellipses and circles) at the seven GPS stations, comparing with the corresponding displacements (open arrows and vertical bars) calculated from the estimated aseismic slip distribution in Fig. 7. Thick upward and downward vertical bars standing at an open square (station location) represent the uplift and subsidence, respectively. The scale of the vertical displacements is the same as that of the horizontal ones.

located along the coast. The horizontal displacements at CAYA and ACAP are 5.2 and 3.5 cm, respectively, and the horizontal displacement at IGUA is almost the same as that at ACAP. The vertical component indicates uplift at three stations located along the coast. From these results, the aseismic slow slip event is considered to occur over a relatively extensive area on the plate boundary between the North America and the Cocos plates, and the amount of slips varies both in the strike and dip directions on the plate interface.

### 3. Method and model of GPS data inversion

In order to obtain spatial distributions of the interplate coupling during the interseismic period and the slow slip event on the plate boundary, we employ an inversion method using a Bayesian information criterion (ABIC) developed by Yabuki and Matsu'ura (1992). Here we use the term back-slip, which is used as the same meaning as slip deficit, to represent inter-

plate coupling (Savage, 1983). Yabuki and Matsu'ura (1992) investigated coseismic slip distribution associated with two large subduction thrust earthquakes, the 1944 Tonankai ( $M$  8.0) and the 1946 Nankai ( $M$  8.1) earthquakes, which occurred in southwest Japan, assuming that the slip distribution is smooth to some degree on a 3-D curved plate boundary in a semi-infinite perfect elastic body. An optimal smoothness was determined objectively and uniquely, using the ABIC proposed by Akaike (1980). The fundamental concept and theory are the same as described in the inversion of the time series data in Section 2.2. Following Yabuki and Matsu'ura (1992), this inversion method has been applied to geodetic data during interseismic periods to estimate back-slip rates on the plate boundaries along several subduction zones around the Japanese Islands (e.g., Yoshioka et al., 1993, 1994; Sagiya, 1999; Ito et al., 1999, 2000; Nishimura et al., 2000). Since detailed and brief explanations are described in these papers, we do not repeat the inversion method here. The only difference between the present and previous stud-

ies is a basis function which was used to represent slip distributions. In the previous papers, bi-cubic B-spline function was used, while we employed a box-car function in this study, assuming a uniform slip for each segment on a model region. An advantage of the latter is that we can reduce the number of unknown parameters. In this study, a weight of data for each component is given so that it can be inversely proportional to its standard deviation calculated in Section 2.2. Therefore, the horizontal data are considered more important than the vertical data in our inversion.

The model region is taken on a 3-D curved plate boundary between the subducting Cocos plate and the overriding North America plate. The geometry is taken from isodepth contours of the subducted oceanic slab by Pardo and Suárez (1995) based on shallow to intermediate-depth seismicity, as shown in Fig. 6. The strike of the model region is taken nearly parallel to the trench axis, and the length and width are taken as 675 and 210 km, respectively. The upper rim of the model region is taken at a depth of about 12 km (a horizontal distance of about 40 km from the trench in the

central part of the model region) in such a way that it can fit the upper rims of the seismogenic zone based on aftershock distributions of megathrust earthquakes and the distributions of medium-size earthquakes that occurred in the Mexican subduction zone. The lower rim is taken at a depth of about 60 km, taking into account possible interplate coupling or slow slip event extending down to the depth. Locations of the two side rims of the model region are taken to cover the northwestern and southeastern ends of the GPS stations. We took the same model region in our GPS data inversion both for interplate coupling during the interseismic period and for the aseismic slow slip event. It should be noted that the outside of the model region is assumed to be decoupled during the interseismic period and locked completely for the aseismic event, respectively. We divided the curved model region into nine (or 25) segments equidistantly, and attempted to estimate two slip components in the strike and dip directions. In this case, the number of unknown parameters to be determined is 18 (or 50) for 21 data in the interseismic period and 17 data in the slow slip event,

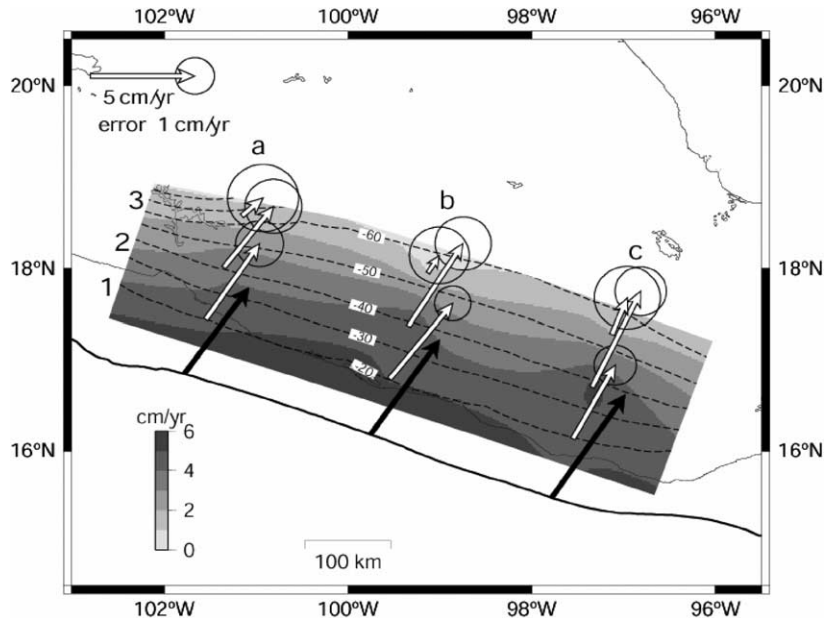


Fig. 6. Back-slip rates and their directions (open arrows) with their estimation errors ( $1\sigma$ , thick black circles) at nine ( $3 \times 3$ ) segments of the model region on the 3-D curved plate interface. The isodepth contours taken from Pardo and Suárez (1995) are represented by dashed lines with 10 km interval. Solid vectors denote the convergence velocity and their directions of the Cocos plate relative to the North America plate along the Middle America trench. The amounts of back-slips, which are uniform within each segment, are smoothed spatially and denoted by gray-scale contours with 1 cm/year interval.

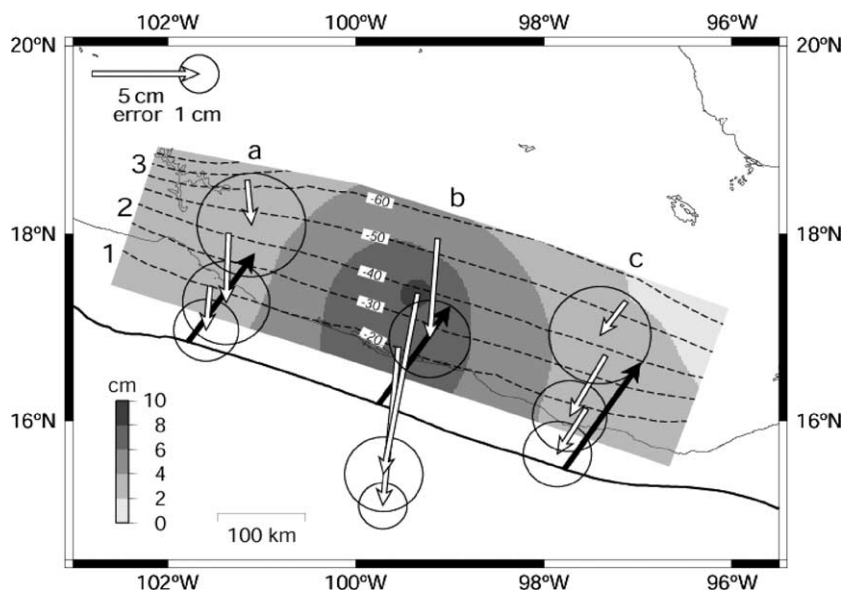


Fig. 7. Spatial distribution of slow slips (open arrows) with their estimation errors ( $1\sigma$ , black circles) at the nine ( $3 \times 3$ ) segments of the model region on the 3-D curved plate interface. The amounts of slow slips, which are uniform within each segment, are smoothed spatially and denoted by gray-scale contours with 2 cm interval. Others are the same as Fig. 6.

respectively (Figs. 4 and 5, Table 1). In order to indicate the location of each segment on the model region, letters *a*, *b*, and *c* and numbers 1, 2, and 3 are given in Figs. 6 and 7 along the strike and dip directions, respectively. For instance, the shallowest and north-westernmost segment is denoted as (*a*, 1), which is similar to a 2-D array representation.

In the following sections, we will first show the results from the inversion analysis. As a second step, we will test the robustness of the inversion results and also check if there is any other possible solutions based on some forward modeling. This is because there may be some resolution problems due to the limited number of the available observed data.

## 4. Results and discussion

### 4.1. Interplate coupling during the interseismic period inferred from the inversion

Fig. 6 demonstrates the back-slip rates at the nine segments on the model region, which are obtained from inversion of the GPS data during the interseis-

mic period in Fig. 4. Estimation error calculated from the formula by Jackson and Matsu'ura (1985) is also shown as a circle, centering at the arrow head of each back-slip rate vector in Fig. 6. We find that the back-slip rates are oriented northeastward on all the segments. The average direction of the back-slip rates is  $N31.3^\circ E \pm 5.6^\circ$ , excluding segments having estimation errors larger than the obtained back-slip rates, namely, (*a*, 3) and (*b*, 3) segments. The back-slip rates at the shallowest and middle-depth segments range from 3.9 to 5.4 cm/year.

The solid arrows along the Middle America trench in the figure represent the convergence rates between the Cocos and the North America plates based on the Euler pole of the global plate motion model NUVEL-1A (DeMets et al., 1994). In this region, the average convergence direction of the three vectors is  $N34.9^\circ E$ . The convergence rate increases southeastward gradually, taking values from 5.3 to 6.3 cm/year.

Comparing the calculated back-slip rates with the convergence rates, we find that the average direction of the back-slip rates almost coincides with that of the convergence rates within a range of  $1\sigma$ . Coupling ratio, which is defined by the ratio of the back-slip

rate to the convergence rate, takes a value larger than 0.67 on the shallowest and middle-depth segments, and reaches 0.83–0.86 if (*a*, 2) and (*c*, 1) segments are excluded, indicating very strong interplate coupling down to a depth of about 45 km.

The back-slip rates at the middle-depth segments appear to increase toward the southeastern segments. This may be related to the facts that both the convergence rate and the distance to the volcanic front from the trench axis increase southeastward.

Although the ratios of the estimation errors to the amount of back-slip rates become large at the deepest segments, we find dramatic decrease in the back-slip rate with increasing depth. The decrease of interplate coupling around a depth of about 45 km may be due to high temperature there.

In Fig. 4, we compare the displacement rates calculated from the inverted slip rate distribution in Fig. 6 with the observed rates. The agreement between them is rather good, especially for their horizontal components at four stations located along the Pacific coast. There are a few stations where the observed vertical components are not explained well by our model. Since we introduce an optimal smoothness for the spatial distribution of the back-slip rates, and also smaller weights on the vertical data than on the horizontal data, this disagreement may be regarded as observation errors in the data.

In order to check segment-size dependence on the distribution, we also tested a GPS data inversion with  $5 \times 5$  segments on the same model region. Almost the same results were obtained (not shown here) as those described above, although estimation errors increased by 20–30% on average due to the increase of unknown parameters for this new inversion.

In addition, in order to check the effect of the assumed configuration of the plate interface on the back-slip rate vectors, we carried out another inversion based on the fault geometry adopted in Iglesias et al. (2004), in which two planar faults are connected with a dip of  $17^\circ$  up to a distance of 100 km from the trench and a dip of  $2^\circ$  for the deeper subhorizontal part, covering a similar model region with a dimension of  $675 \text{ km} \times 210 \text{ km}$ . The obtained back-slip rate vectors are almost the same as those described in this section, indicating that the effect of the assumed configuration of the plate interface is almost negligible as far as we use the geometry in Iglesias et al. (2004).

#### 4.2. Slip distribution of the aseismic slow slip event inferred from the inversion

Slip distribution associated with the aseismic slow slip event for  $3 \times 3$  segment model is shown in Fig. 7, and the observed and calculated displacements at the GPS stations are compared in Fig. 5. Agreement between these displacements is found to be acceptable, but not so good as in the case of the back-slip rates, especially for the stations along the coast. It was found that the amount of slip is large at the (*b*, 1) and (*b*, 2) segments, taking values of 7.8 and 9.0 cm, respectively. The slow slip occurs at the deepest segment (*b*, 3) as well. Although estimation errors are relatively large on the *a* and the *c* segments, we find that the amount of slip on these segments is much smaller than on the *b* segment, and that their slip directions are pointed towards those for the *b* segment. The average slip direction except (*a*, 3) and (*c*, 3) segments is not necessarily oriented in the direction opposite to the plate convergence, with the difference of about  $22.7^\circ \pm 4.7^\circ$ . Incidentally, even if we adopted an uplift of 9.3 cm at CAYA, which was described in Section 2.2, for the inversion, the obtained slip distribution was almost the same as Fig. 7, and the calculated uplift at CAYA was also nearly the same as that in Fig. 5. This indicates that the large uplift is not consistent with other estimated values of displacements, and might be produced by some other unknown factors.

When we divided the model region into  $5 \times 5$  segments, instead, almost the same results were obtained as shown in Fig. 8, with somewhat larger estimation errors. In this case, we find similar slip distribution on the *b'* and *c'* segments as that on the *b* segment in Fig. 7 from their shallowest (1') to the deepest (5') ones. These results may be related to the time lag of the slow slip event: displacements associated with the slow slip event started first some time during mid-November to early December 2001 at CAYA, ACAP, IGUA, and YAIG, and then during mid-January to mid-February 2002 at ZIHP, PINO, and OAXA, indicating bilateral propagation of the aseismic slow slip along the direction parallel to the trench axis (Kostoglodov et al., 2003). A similar propagation along the trench parallel direction (but with unilateral propagation) of an aseismic slow slip has also been detected by a continuous GPS network in the Cascadia subduction zone (Dragert et al., 2001). The seismic moment is esti-

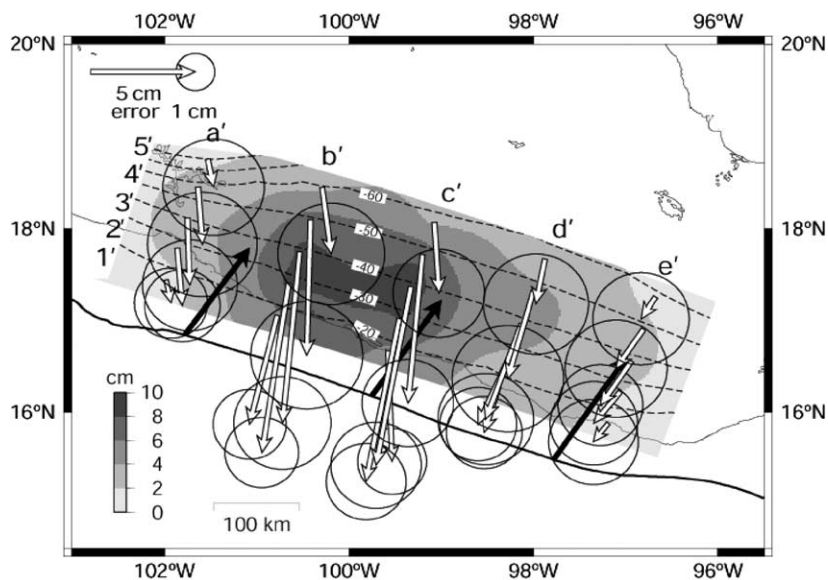


Fig. 8. Spatial distribution of slow slips (open arrows) with their estimation errors ( $1\sigma$ , black circles) at 25 ( $5 \times 5$ ) segments of the model region on the 3-D curved plate interface. Others are the same as Fig. 7.

mated to be  $1.6 \times 10^{20}$  Nm, equivalent to  $M_w = 7.4$  when we sum up the effects of all segments whose amounts of slips are larger than the estimation errors in Fig. 8.

The effect of configuration of the plate interface was also investigated, as in the previous section for combinations of the two planar planes, assuming the fault geometry by Iglesias et al. (2004). However, we cannot find any systematic differences, indicating that our results do not depend on the geometry.

#### 4.3. Estimate of the depth ranges of interplate coupling and the slow slip from forward modeling

In the inversion described above, we had to restrict our calculations on a small number of segments with  $3 \times 3$  or  $5 \times 5$  with uniform slip in each segment, because of the limited number of data. In this section we perform some forward modeling for  $9 \times 9$  segments, to check the robustness of the inversion results.

We first assigned a uniform back-slip with the same amplitude and direction as those calculated from the plate motion model (NUVEL-1A), from the upper rim down to a depth of about 30 km along the entire model length (675 km). In this case we found that while the displacement rates observed at the four coastal stations

can be roughly explained by the assigned back-slip distribution, the calculated rates for the rest three inland stations are too small to explain the observed ones. On the other hand, assuming a similar uniform slip down to a depth of 47 km as in Model A in Fig. 9(a), the observed displacements at all the seven stations can be well explained. These results suggest that the interplate coupling may achieve the depth of about 45 km, which is consistent with the back-slip distribution obtained by the inversion (Fig. 6). An alternative model with a gradual decay of the rates in the transition zone (Model B in Fig. 9(a)) would also fit well all the observations. It is to be mentioned, however, that such a depth profile as in Model B is quite different from that in the Cascadia subduction zone, where the back-slip decreases more gradually with depth (Wang et al., 2003).

Similar forward modeling is performed for the slip distribution associated with the aseismic slow slip event. To check the depth extent of the slow slip inland from the Guerrero region more carefully, our forward modeling is focused on four stations aligned perpendicularly to the trench axis in this region (Fig. 10(b)). If we assume a uniform slip of 9 cm in the direction of  $32^\circ$  counterclockwise from the opposite direction of the plate convergence, from the upper rim down to

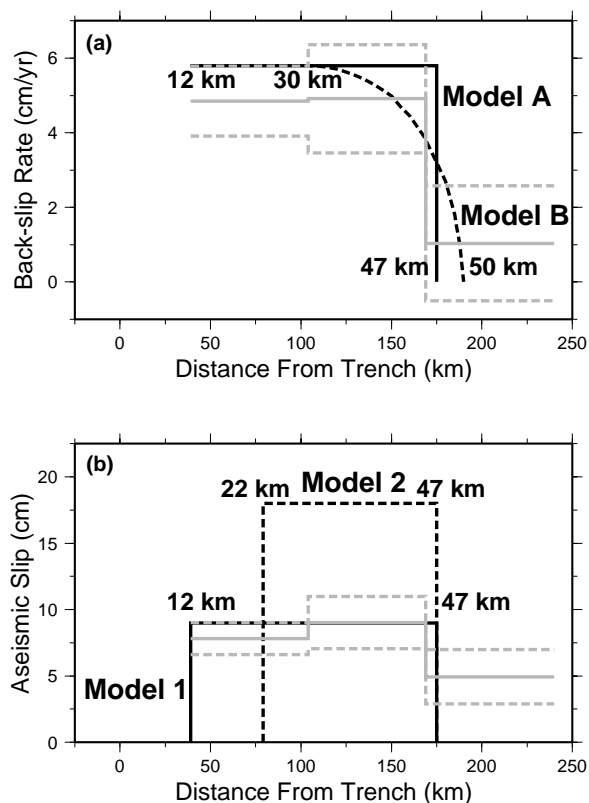


Fig. 9. (a) Possible range of the back-slip rates estimated as a function of the horizontal distance from the trench axis. Gray solid and dashed lines indicate the rate and its uncertainty ( $1\sigma$ ) estimated from the inversion analysis, respectively, along the *b* segment in Fig. 6. Black solid line (Model A) and dashed curve (Model B) show the back-slip rates estimated from forward modeling. (b) Possible range of aseismic slip as a function of the horizontal distance from the trench axis. Gray solid and dashed lines indicate the aseismic slip and its uncertainty ( $1\sigma$ ) estimated from the inversion, respectively, along the *b* segment in Fig. 7. Black solid (Model 1) and dashed (Model 2) lines show the aseismic slip estimated from forward modeling.

a depth of 47 km as in Model 1 in Fig. 9(b), the observed displacements at these four stations are rather well explained, indicating that the inversion results in Figs. 7 and 8 are supported from this test. For a next attempt, varying the up-dip depth of the slip region and fixing the down-dip limit at 47 km, we found that for the increase of the depth of up-dip limit, larger amount of slow slip is required to fit the observed surface displacements. Fig. 10 denotes the case when a uniform slip of 18 cm is assumed for the depth from

22 to 47 km in the middle of the model region (Model 2 in Fig. 9(b)). The reason for this larger slip is that the two coastal stations, CAYA and ACAP, with the largest seaward horizontal displacements, are located outside of the slip region. However, if we take shallower down-dip depth limit, fixing the up-dip depth at 22 km, the displacement observed at the two coastal stations cannot be explained, even if much larger slip is assumed.

On the other hand, if the slip region has the up-dip limit deeper than about 25 km, the situation becomes quite different. Since the up-dip limit of the slip region is far away from CAYA and ACAP, much larger slip is required to explain the observed displacements at the two stations, but the seaward horizontal displacements calculated for two inland stations IGUA and YAIG become too large. In this case, therefore, there is not a simple solution to explain the observations at the four stations simultaneously.

From these forward modeling tests, we can conclude that the slip distributions shown in Figs. 7 and 8 are probable solutions, but it would also be possible to have other solutions with such larger slip at deeper depths as in Model 2 in Fig. 9(b). These conclusions are generally consistent with the results of a 2-D analysis by Kostoglodov et al. (2003). It is to be noted, however, that such large aseismic slip as in Model 2 would release most of the shear stress accumulated at the depth range between 22 and 47 km during the preceding 3 years and a half due to plate coupling, but would generate high stress concentration at depths shallower than 22 km, as discussed in the last section.

#### 4.4. Relation between aseismic slow slip and interplate coupling, and its tectonic implications

A possible strong interplate coupling down to a depth of about 45 km seems to be compatible with a thermal model proposed by Currie et al. (2002), and also with coseismic slip distributions of some large subduction thrust earthquakes in the Mexican subduction zone. Currie et al. (2002) suggested that temperature of 350 °C may control the down-dip extent of the seismogenic zone in Guerrero, which is slightly shallower than a depth of 40 km. On the other hand, the waveform inversion analysis indicates that while the down-dip depth of the coseismic slip ranges from 20 to 30 km for the 1979 Petatlan (Mw 7.6), the 1981

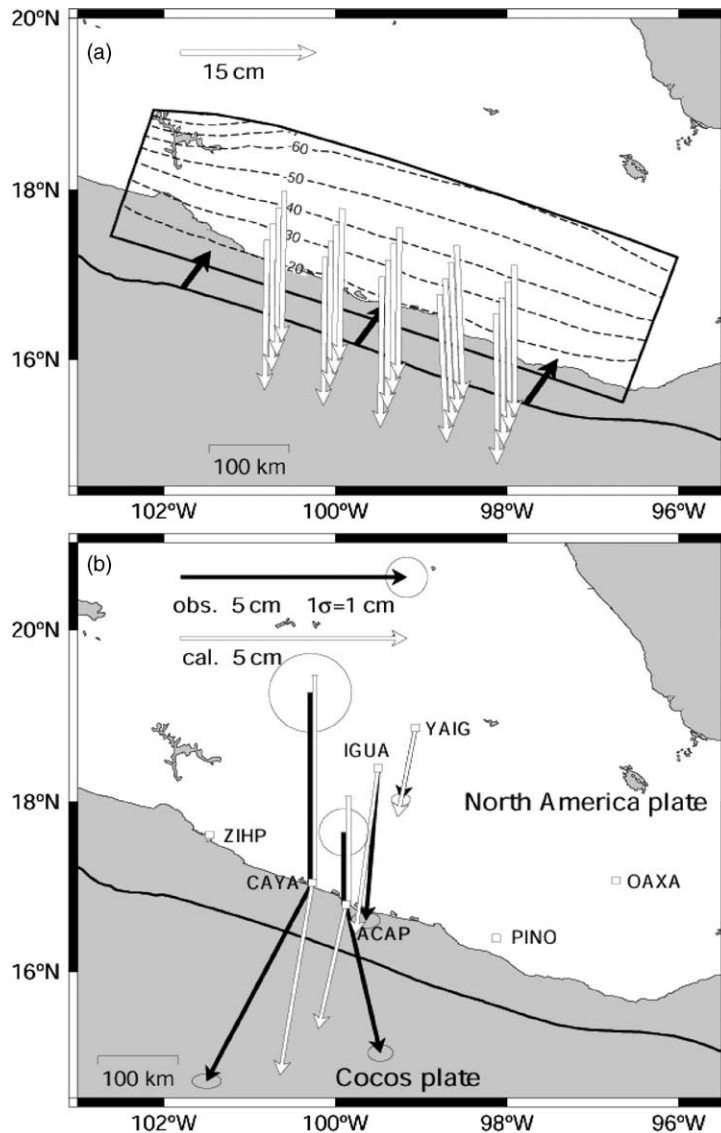


Fig. 10. (a) Assigned uniform slip of 18 cm (open arrows) on the 3-D curved plate interface in the direction of  $32^\circ$  counterclockwise from the opposite direction of the plate convergence in forward modeling (Model 2 in Fig. 9(b)). Solid arrows denote the convergence rates and their directions of the Cocos plate relative to the North America plate along the Middle America trench. The isodepth contours taken from Pardo and Suárez (1995) are represented by dashed lines with 10 km interval. (b) The horizontal (open arrows) and vertical (open vertical bars) displacements calculated from the assigned slip distribution in (a) are compared with the observed displacements (solid arrows and solid vertical bars) associated with the slow slip event with their standard deviations (ellipses and circles) at the four GPS stations. Others are the same as Fig. 5.

Playa Azul (Mw 7.4), and the 1985 Zihuatanejo (Mw 7.7) earthquakes (Mendoza, 1993, 1995), Mendoza and Harzell (1989) and Yagi et al. (in press) estimated a down-dip depth of about 40 km for the 1985 Mi-

choacan (Mw 8.1) and the 2003 Colima (Mw 7.9) earthquakes, respectively. These results suggest that the down-dip depth limit of about 45 km estimated in this study is a reasonable estimate for the coupled zone

in the Mexican subduction zone, although it depends on the geometry of the plate interface.

Comparing the depth extent of the slow slip with that of the back-slip rates in Fig. 9, we found from our inversion and forward modeling that the slow slip appears to have occurred not only on the deeper coupled segments, but also on a strongly coupled region at least up to about 25 km. From these results, we may consider two extreme possibilities. The first possibility is that the slow slip reached a shallower part of the seismogenic zone, up to the up-dip depth of 12 km (Model 1 in Fig. 9(b)). The second possibility is that the slow slip reached a depth of about 25 km, which might be a deeper part of the seismogenic zone. In any case, these modeling results are in favor of the hypothesis that the aseismic slow slip was not limited only within a transition zone, down-dip from the strongly coupled zone, but might have invaded a deeper part of the locked seismogenic zone where a large subduction thrust earthquake is expected to occur some time in the future. Such an aseismic slow slip event with  $M_w = 6.6$  in the seismogenic depth range is also found in the eastern part of the Boso peninsula, central Japan in 2002 (Ozawa et al., 2003).

Here, we consider the deviation of the aseismic slip direction from the opposite direction of plate convergence. To investigate the tectonic regime in the Mexican subduction zone, we plotted 87 Harvard CMT solutions of all the thrust-type subduction earthquakes during the period from June 1976 to February 2004. We found that the slip directions for about half of them are in the opposite direction of the plate convergence, while the slip directions for the rest of the events deviate from the direction by about  $20^\circ$ – $35^\circ$  counterclockwise, which is more or less consistent with our results. From this comparison, it seems that the systematic deviation of the slip direction associated with the slow slip event may not be an unusual feature in the stress release mechanism in this zone.

Large subduction thrust earthquakes ( $M_w > 7$ ) have never occurred in the northwestern Guerrero region since 1911. If we assume that such aseismic slow slip events have occurred episodically as in early 1998 (CAYA in Fig. 2) and in late 2001 to middle 2002, and the slip propagated into a part of the locked seismogenic zone as in the first possibility, the slow slip events would not accelerate the onset of a large subduction earthquake due to stress concentration at the

locked zone, but rather would delay its occurrence due to some stress release, as will be discussed in the next section.

On the other hand, it can be seen from Fig. 1 that large thrust earthquakes have taken place in the shallow section of the adjacent regions northwest and southeast of the Guerrero gap, suggesting large tectonic stress acting on in the shallow seismogenic zone there, unlike in the Guerrero region. There is a possibility that the aseismic slow slip in the adjacent regions remained mainly in a deeper plate interface below this zone more like in Model 2 in Fig. 9(b) but with smaller slip than in Figs. 7 and 8, yielding stress concentration in the shallow section. If this is the case, the slow slip would have spatially more variable distribution than discussed here, while the interplate coupling indicates laterally rather uniform back-slip rates as shown in Fig. 6.

#### 4.5. Shear stress changes associated with interplate coupling and the slow slip event

To discuss the possibility of the occurrence of a future large earthquakes in the Guerrero region, we made simple estimates of the shear stress accumulated during the interseismic period and its change due to the slow slip event. In this case, we approximate the 3-D curved plate interface by a flat surface with an average dip of  $15^\circ$  and with the same dimension of the model region as given in Figs. 6–8. Calculations of shear stress were made based on a simple dislocation model in a 3-D half-space (Okada, 1992). The accumulated shear stress during 3 years and a half from mid-1998 to late 2001 was calculated from the back-slip rates on  $5 \times 5$  segments (not shown here). It is estimated as about 0.025–0.028 MPa on most part of the modeled interface, except the deepest segments ( $a'$ ,  $5'$ )–( $e'$ ,  $5'$ ) (as indicated in Fig. 8) and near the northwestern and southeastern edges.

On the other hand, the stress change due to the slow slip event was calculated from a slip distribution along the  $N34^\circ E$  direction, which has been obtained by a cubic-spline interpolation from Fig. 8 into  $10 \text{ km} \times 10 \text{ km}$  sub-segments. The results from the inversion show that a largest stress decrease of 0.020–0.023 MPa occurs on the deeper part of the ( $b'$ ,  $1'$ ) and ( $c'$ ,  $1'$ ) segments and on the shallower part of the ( $b'$ ,  $2'$ ) and ( $c'$ ,  $2'$ ) segments, with somewhat smaller stress decrease

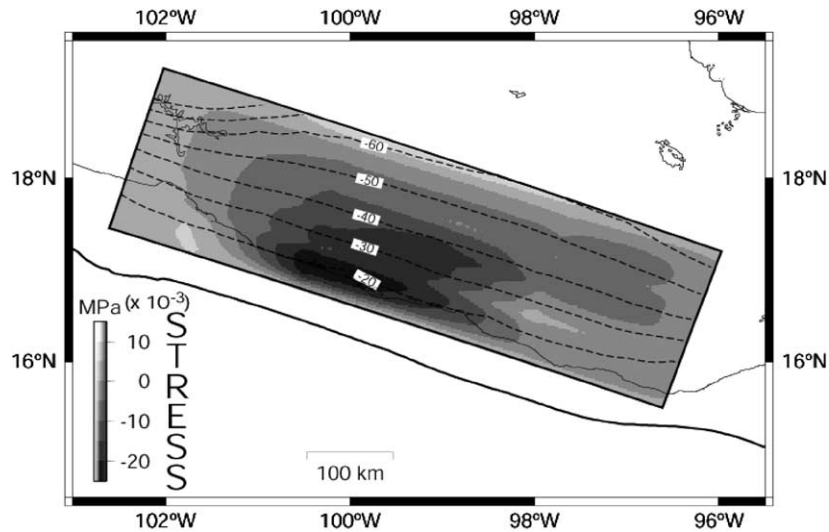


Fig. 11. Spatial distribution of shear stress change, calculated from the slip distribution shown in Fig. 8 by a cubic-spline interpolation into  $10\text{ km} \times 10\text{ km}$  subsegments. The calculations were made for a flat plate interface based on a dislocation model in a 3-D half-space (Okada, 1992). The contour interval for the amount of shear stress is  $5 \times 10^{-3}$  MPa.

of about 0.015–0.018 MPa on the shallower part of the ( $b'$ ,  $3'$ ) and ( $c'$ ,  $3'$ ) segments (Fig. 11). The stress decrease on the peripheral segments is of the order of 0.003–0.005 MPa.

The above estimates indicate that about 80% of the shear stress accumulated since mid-1998 may have been released on the four central segments, while 40–50% of the accumulated stress still remains unreleased on the shallowest segments of the seismogenic zone. This result suggests that the time of occurrence of a future large earthquake may be delayed to some extent or smaller earthquakes would take place by the slow slip event. If, alternatively, the slow slip remained only on the deeper part of the seismogenic zone down from a depth of 22 km as in Model 2 in Fig. 9(b), the shear stress at these depths would decrease down to 0.05 MPa, whereas it would increase up to about 0.01–0.02 MPa in the seismogenic zone above the shallowest segments. In such a case, on the contrary, a future earthquake would occur at a slightly advanced time. Which one of the above two different cases would take place depends on up to what depth the slow slip event actually invaded the seismogenic zone. This issue should be investigated in more detail in the near future after more permanent GPS stations are installed in and around the Guerrero region.

## 5. Conclusions

In this study, we have estimated the displacement rates during the interseismic steady state period and the displacements associated with a slow slip event, from the inversion of the time series data obtained at seven continuous GPS stations located in and around the Guerrero region. We carried out the inversion analysis with an application of the ABIC and some forward modeling on a 3-D curved plate interface to estimate spatial distribution of the back-slip rates and the slip of the aseismic slow slip event. Significant conclusions obtained in this study are as follows:

- (1) The average direction of the inverted back-slip rates ( $N31.3^\circ E \pm 5.6^\circ$ ) almost coincides with the average direction of plate convergence of the subducting Cocos plate relative to the continental North America plate ( $N34.9^\circ E$ ). The coupling ratio on the shallowest and middle-depth segments except the two segments ( $a$ , 2) and ( $c$ , 1) in Fig. 6 ranges from 0.83 to 0.86, indicating very strong interplate coupling down to a depth of about 45 km, for the subducting slab geometry from Pardo and Suárez (1995). At depths deeper than about 45 km, the state of coupling becomes weaker dramati-

cally due to high temperatures there (Currie et al., 2002). The amount of the back-slip rates at the middle-depth segments appears to increase toward southeast. This may be related to the facts that both the convergence rate and the distance to the volcanic front from the trench axis increase south-eastward. The average direction of the slow slip is oriented about  $20^{\circ}$ – $35^{\circ}$  counterclockwise from the opposite direction of the plate convergence, which might be related to some stress release mechanism or seismotectonic regime inherent in this region.

- (2) Slip distribution associated with the aseismic slow slip event indicates large slips on the central (*b*, 1) and (*b*, 2) segments in Fig. 7, reaching 7.8 and 9.0 cm, respectively. From the detailed analysis by the inversion and forward modeling, it was found that the slow slip might reach at least some depth shallower than about 25 km. Unlike the results from the most previous studies of slow slip events, our analysis suggests that the slow slip may have occurred not only on a transition zone below the seismogenic zone, but also on a deeper part of the locked seismogenic zone. Simple stress calculations suggest that if these slow slip events occur episodically, possible occurrence of a forthcoming large earthquake in the Guerrero seismic gap would be delayed for some time or smaller coseismic slip would be expected. If, however, the slow slip remained only in the deeper part below the locked seismogenic zone, a future earthquake would occur at a slightly advanced time than expected.

## Acknowledgements

We are grateful to T. Yabuki for sharing his original source code for geodetic data inversion. We thank Jose Antonio Santiago and Jose Luis Cruz (IGEF, UNAM) for the installation and maintenance of the GPS stations. The GPS continuous data are archived at UNAVCO (CAYA station) and at SOPAC (YAIG station). Yehuda Bock inspired the installation of GPS station at Yautepec (YAIG), and provided the equipment. T. Sagiya, D. Gubbins, and an anonymous reviewer are acknowledged for their critical comments to improve the manuscript. We also thank A. Iglesias for some discussion in this study, and T. Ito for his kind help with

the calculation. All the figures were created using the Generic Mapping Tools (GMT) software (Wessel and Smith, 1995). This study is partly supported by NSF to the University of Colorado, EAR-9725712 and EAR 0125618, and by the CONACyT (Mexico) project no. 41209-F.

## References

- Akaike, H., 1980. Likelihood and the Bayes procedure. In: Bernardo, J.M., DeGroot, M.H., Lindley, D.V., Smith (Eds.), *Bayesian Statistics*. University Press, Valencia, Spain, pp. 143–166.
- Boucher, C., Altamini, Z., Sillard, P., 1999. The 1997 International Terrestrial Reference Frame (ITRF97). IERS Tech. Notes 27. Int. Earth Rotation Service, Paris.
- Currie, C.A., Hyndman, R.D., Wang, K., Kostoglodov, K., 2002. Thermal models of the Mexico subduction zone: implications for the megathrust seismogenic zone. *J. Geophys. Res.* 107, doi: 10.1029/2001B000886.
- DeMets, C., Gordon, R.G., Argus, D.F., Stein, S., 1994. Effect of recent revisions to the geomagnetic reversal time scale on estimates of current plate motion. *Geophys. Res. Lett.* 21, 2191–2194.
- Dragert, H., Wang, K., James, T.S., 2001. A silent slip event on the deeper Cascadia subduction interface. *Science* 292, 1525–1528.
- Hirose, H., Hirahara, K., Kimata, F., Fujii, N., Miyazaki, S., 1999. A slow thrust slip event following the two 1996 Hyuganada earthquakes beneath the Bungo Channel, southwest Japan. *Geophys. Res. Lett.* 26, 3237–3240.
- Iglesias, A., Singh, S.K., Lowry, A., Santoyo, M.A., Kostoglodov, V., Larson, K.M., Franco-Sánchez, S.I., Mihumo, T., 2004. The silent earthquake of 2002 in the Guerrero seismic gap, Mexico (Mw = 7.6): inversion of slip on the plate interface and some implications. *Geofísica Int.* 43, 309–317.
- Ito, T., Yoshioka, S., Miyazaki, S., 1999. Interplate coupling in southwest Japan deduced from inversion analysis of GPS data. *Phys. Earth Planet. Interiors* 115, 17–34.
- Ito, T., Yoshioka, S., Miyazaki, S., 2000. Interplate coupling in northeast Japan deduced from inversion analysis of GPS data. *Earth Planet. Sci. Lett.* 176, 117–130.
- Jackson, D.D., Matsu'ura, M., 1985. A Bayesian approach to nonlinear inversion. *J. Geophys. Res.* 90, 581–591.
- Kostoglodov, V., Singh, S.K., Santiago, J.A., Franco, S.I., Larson, K., Lowry, A., Bilham, R., 2003. A large silent earthquake in the Guerrero seismic gap, Mexico. *Geophys. Res. Lett.* 30, doi: 10.1029/2003GL017219.
- Larson, K.M., Kostoglodov, V., Lowry, A., Hutton, W., Sanchez, O., Hudnut, K., Suárez, G., 2004. Crustal deformation measurements in Guerrero, Mexico. *J. Geophys. Res.*, in press.
- Lichten, S., Border, J., 1987. Strategies for high precision GPS orbit determination. *J. Geophys. Res.* 92, 12751–12762.
- Lowry, A.R., Larson, K.M., Kostoglodov, V., Bilham, R., 2001. Transient fault slip in Guerrero, southern Mexico. *Geophys. Res. Lett.* 28, 3753–3756.

- Mendoza, C., 1993. Coseismic slip of two large Mexican earthquakes from teleseismic body waves: implications for asperity interaction in the Michoacan plate boundary segment. *J. Geophys. Res.* 98, 8197–8210.
- Mendoza, C., 1995. Finite-fault analysis of the 1979 March 14 Petatlan, Mexico, earthquake using teleseismic P waveforms. *Geophys. J. Int.* 121, 675–683.
- Mendoza, C., Harzell, S., 1989. Slip distribution of the 19 September 1985 Michoacan, Mexico, earthquake: near-source and teleseismic constraints. *Bull. Seismol. Soc. Am.* 79, 655–669.
- Nishimura, T., Miura, S., Tachibana, K., Hashimoto, K., Sato, T., Hori, S., Murakami, E., Kono, T., Nida, K., Mishina, M., Hirasawa, T., Miyazaki, S., 2000. Distribution of seismic coupling on the subducting plate boundary in northeastern Japan inferred from GPS observations. *Tectonophysics* 323, 217–238.
- Okada, Y., 1992. Internal deformation due to shear and tensile faults in a half space. *Bull. Seism. Soc. Am.* 82, 1018–1042.
- Ozawa, S., Miyazaki, S., Hatanaka, Y., Imakiire, T., Kaidzu, M., Murakami, M., 2003. Characteristic silent earthquakes in the eastern part of the Boso peninsula, central Japan. *Geophys. Res. Lett.* 30, doi: 10.1029/2002GL016665.
- Ozawa, S., Murakami, M., Kaizu, M., Tada, T., Sagiya, T., Hatanaka, Y., Yurai, H., Nishimura, T., 2002. Detection and monitoring of ongoing aseismic slip in the Tokai region, central Japan. *Science* 298, 1009–1012.
- Ozawa, S., Murakami, M., Tada, T., 2001. Time-dependent inversion study of the slow thrust event in the Nankai trough subduction zone, southwestern Japan. *J. Geophys. Res.* 106, 787–802.
- Pardo, M., Suárez, G., 1995. Shape of the subducting Rivera and Cocos plates in southern Mexico. *J. Geophys. Res.* 100, 12357–12373.
- Sagiya, T., 1999. Interplate coupling in the Tokai district, central Japan, deduced from continuous GPS data. *Geophys. Res. Lett.* 26, 2315–2318.
- Savage, J.C., 1983. A dislocation model of strain accumulation and release at a subduction zone. *J. Geophys. Res.* 88, 4984–4996.
- Singh, S.K., Mortera, F., 1991. Source-time functions of large Mexican subduction zone earthquakes, morphology of the Benioff zone, age of the plate and their tectonic implications. *J. Geophys. Res.* 96, 21487–21502.
- Suárez, G., Monfret, T., Wittlinger, G., David, C., 1990. Geometry of subduction and depth of the seismogenic zone in the Guerrero gap, Mexico. *Nature* 345, 336–338.
- Tanabe, K., 1985. A Bayesian model and ABIC. *Operat. Res.*, 178–183 (in Japanese).
- Wang, K., Wells, R.E., Mazzotti, S., Hyndman, R.D., Sagiya, T., 2003. A revised dislocation model of interseismic deformation of the Cascadia subduction zone. *J. Geophys. Res.* 108, doi: 10.1029/2001JB001227.
- Wessel, P., Smith, W.H.F., 1995. New version of the Generic Mapping Tools released. *EOS Trans. AGU* 76, 329.
- Yabuki, T., Matsu'ura, M., 1992. Geodetic data inversion using a Bayesian information criterion for spatial distribution of fault slip. *Geophys. J. Int.* 109, 363–375.
- Yagi, Y., Mikumo, T., Pacheco, J., Reyes, G. Source rupture process of the Tecoman, Colima, Mexico earthquake of January 22, 2003, determined by joint inversion of teleseismic body wave and near-source data. *Bull. Seismol. Soc. Am.*, in press.
- Yoshioka, S., Yabuki, T., Sagiya, T., Tada, T., Matsu'ura, M., 1993. Interplate coupling and relative plate motion in the Tokai district, central Japan, deduced from geodetic data inversion using ABIC. *Geophys. J. Int.* 113, 607–621.
- Yoshioka, S., Yabuki, T., Sagiya, T., Tada, T., Matsu'ura, M., 1994. Interplate coupling in the Kanto district, central Japan, deduced from geodetic data inversion and its tectonic implications. *Tectonophysics* 229, 181–200.